Simulation of an adhesive layer using a novel mixed mode cohesive law

J.L. Högberg[1] and K. Salomonsson
Mechanics of materials, University of Skövde, Box 408, SE-541 28, Sweden

Abstract

The purpose of this work is to develop a flexible cohesive law to simulate the constitutive behaviour of an adhesive layer under mixed mode loading. A mixed mode cohesive law that captures the linear elastic and softening behaviour before fracture is presented. This simple model uses a coupled formulation to describe the mixed mode cohesive behaviour. It also allows for different fracture parameters, such as fracture energy, strength and critical separation in different mode mixities. Thus, the fracture process in mode I (peel), in mode II (shear) or in mixed mode (a combination of peel and shear) can be modelled without the usual constraint of a common fracture energy in peel and shear. Examples are given of FE-implementation of the normalised cohesive law, namely for the Unsymmetric Double Cantilever Beam (UDCB) specimen and the Mixed-mode double Cantilever Beam (MCB) specimen. Both specimens are adhesively bonded and loaded in mixed-mode.

Keyword: cohesive law, fracture energy, traction-separation relation, mixed mode

1. Introduction

In usage, adhesives are constrained between the bodies and are thus thin layers. An adhesive as a thin layer behaves differently in comparison to the adhesive as a bulk material. Although the thickness of the adhesive layer is small in comparison to the overall dimension of the joint, the size of the thickness influences the mechanical properties of the joint (Högberg, 2004).

Experimental studies show that a moderately ductile adhesive layer is much stronger in shear than in peel. Mode I experiments in peel have been conducted with a symmetric DCB-specimen, in which two steel adherends are bonded by a thin layer (t = 0.2 mm) of the structural adhesive DOW Betamate XW1044-3 (Andersson and Stigh, 2004). To concentrate on the nonlinear properties of the adhesive layer, the adherends are dimensioned to remain elastic under quasi-static loading. Mode II experiments in shear have been conducted in a similar manner with an ENF-specimen (Leffler et al., 2006). Based on the J integral (Rice 1968), the constitutive relations of the adhesive layer in peel and in shear are evaluated. The results show that the strength in shear is approximately 26 MPa, which is larger than the 20 MPa in peel, and the fracture energy in shear is approximately 2300 N/m, which is about three times larger than in peel (760 N/m). Similar results are observed by other researchers, e.g. Chai, 2003; Sørensen et al., 2004; Li et al., 2006.

The fracture energy for an adhesive layer comprises the intrinsic energy as well as the energy due to plastic dissipation. In numerical applications, there are mainly three techniques for modelling an adhesive layer:

1. The adhesive layer is modelled as an *interface* between the joined bodies, by which the effect due to the thickness of the layer is ignored. (Pantano and Averill, 2004)
2. The layer is modelled as an elastoplatic *continuum* with fracture parameters, which combines material parameters of the adhesive as a bulk material together with a traction-separation relation with fracture parameters. (Tvergaard and Hutchinsson, 1996; Pardoen et al., 2005)
3. The *layer* is modelled as an interphase with a thickness. A cohesive law that describe the macroscopic response of the layer is used. (Kafkalidis and Thouless, 2002; Salomonsson, 2002)

[1]Corresponding author. Tel: +46 (0)500 448543; fax: +46 (0)500 448549;
E-mail: li.hogberg@his.se

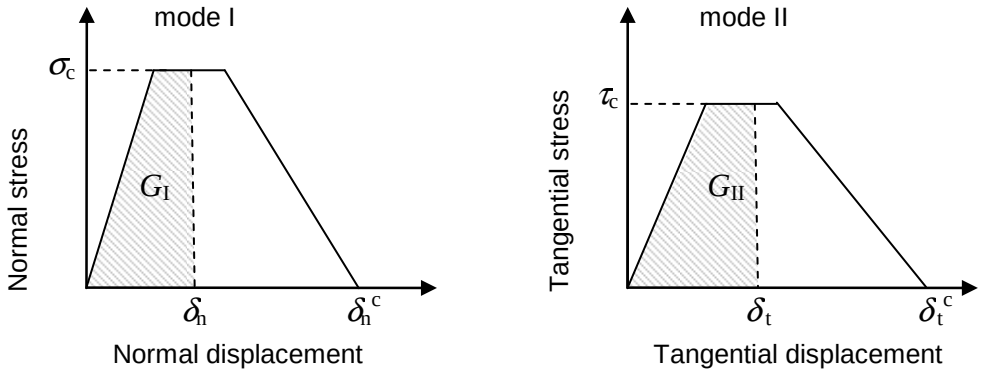

Figure 1 An uncoupled approach: Embedded Process Zone model
used in numerical studies by Thouless and co-workers.

The layer technique (3) is a good compromise of techniques (1) and (2), which is much simpler than the continuum technique (2) but the result is more accurate than the layer technique (1).

In this paper, a flexible cohesive law to simulate the constitutive behaviour of an adhesive layer under mixed mode loading is presented in chapter 2. For FE-implementation, interphase elements are developed and given in Chapter 3. Finally, examples in simulation of adhesive joints by using the layer technique (3) are given for the Unsymmetric Double Cantilever Beam (UDCB) specimen and the Mixed-mode double Cantilever Beam (MCB) specimen.

2 Mixed mode cohesive law

The concept to describe the cohesive activities before fracture has been established for half a century by Barrenblatt (1962). These days, cohesive laws are usually associated with cohesive zone modelling in the numerical simulation of the fracture process. Due to its simplicity, cohesive laws are used for a wide variety of applications. For analysing mixed mode fracture processes, two approaches are used: uncoupled and coupled cohesive zone modelling. For example, Thouless and co-workers simulate a mixed-mode loaded adhesive layer, with a so called *Embedded Process Zone* (EPZ) model, cf. Fig 1. The stress-deformation relations in mode I (peel) and mode II (shear) are assumed uncoupled under mixed mode loading cases. The energy release rate (ERR) in mode I (G_I) and mode II (G_{II}) are identified as the areas under the respective EPZ-curves, and the total ERR is the sum of the ERR in mode I and II. The fracture criteria is energy based, which can cause sudden drops in the tractions before the critical separation is reached. (Kafkalidis and Thouless, 2002; Li et al., 2006)

A frequently used coupled cohesive law is developed by Tvergaard and Hutchinson (1992). This T-H model uses a dimensionless separation parameter, $\lambda = \left[(\delta_n / \delta_n^c)^2 + (\delta_t / \delta_t^c)^2\right]^{1/2}$, to couple the peel and shear modes. Here, δ_n and δ_t are the normal and the tangential separation, respectively. The traction increases with λ to a plateau, then decreases linearly until fracture, cf. Fig 2. A drawback with this model is that the fracture energy is the same in all mode mixities. This cohesive law is thought to model the intrinsic fracture process within a material or along an interface of two solids. It is usually

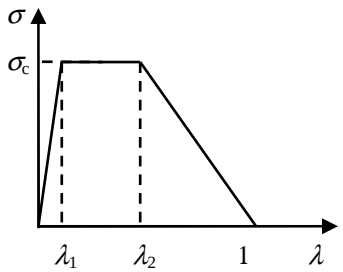

Figure 2 The coupled cohesive law by Tvergaard and Hutchinson.

complemented by constitutive models of the surrounding continua. (Tvergaard and Hutchinson, 1996; Pardoen et al., 2005; Salomonsson and Andersson, 2006)

A mode dependent mixed mode cohesive law with coupled formulation is proposed by Högberg (2006). It uses a dimensionless deformation measure λ as the coupling parameter, which is defined by

$$\lambda^2 = \bar{v}^2 + \bar{w}^2 = \left(\frac{v}{v_c}\right)^2 + \left(\frac{w}{w_c}\right)^2 \tag{1}$$

where $\bar{w}$ and $\bar{v}$ are the normalised normal and tangential deformation, respectively. Softening behaviour of the adhesive layer begins when $\lambda = \lambda_p$, which is given by

$$\lambda_p^{\,2} = \frac{\bar{v}_p^2\,\bar{w}_p^{\,2}}{\bar{v}_p^{\,2}\sin^2\theta + \bar{w}_p^{\,2}\cos^2\theta} \tag{2}$$

where $\theta = \tan^{-1}(\bar{w}/\bar{v})$. For each value of θ, the normalised stress, *S*, is defined by

$$S(\lambda,\theta) = \begin{cases} \dfrac{\lambda}{\lambda_p(\theta)} & \text{when} \quad 0 < \lambda \le \lambda_p \\ \dfrac{1-\lambda}{1-\lambda_p(\theta)} & \text{when} \quad \lambda_p < \lambda \le 1 \\ 0 & \text{when} \quad \lambda > 1 \end{cases} \tag{3}$$

This is shown schematically in Fig. 3. The normalised ERR is defined as the area under the normalised stress curve *S*

$$\bar{J}(\lambda,\theta) = \int_0^{\lambda} S(\tilde{\lambda})\,\mathrm{d}\tilde{\lambda} = \int_0^{\bar{w}} \frac{S}{\tilde{\lambda}}\tilde{\bar{w}}\,\mathrm{d}\tilde{\bar{w}} + \int_0^{\bar{v}} \frac{S}{\tilde{\lambda}}\tilde{\bar{v}}\,\mathrm{d}\tilde{\bar{v}} = \bar{J}(\bar{w},\bar{v}) \tag{4}$$

Decomposition of the normalised ERR is based on the deformation in mode I and mode II directions, i.e.

$$\bar{J}_{\mathrm{I}} = \int_0^{\bar{w}} \frac{S}{\tilde{\lambda}}\tilde{\bar{w}}\,\mathrm{d}\tilde{\bar{w}}, \qquad \bar{J}_{\mathrm{II}} = \int_0^{\bar{v}} \frac{S}{\tilde{\lambda}}\tilde{\bar{v}}\,\mathrm{d}\tilde{\bar{v}} \tag{5a, b}$$

The ERR gains a physical meaning by multiplication with the characteristic cohesive parameters

$$J_{\mathrm{I}} = \sigma_c w_c \bar{J}_{\mathrm{I}} = 2J_{\mathrm{Ic}}\bar{J}_{\mathrm{I}}, \qquad J_{\mathrm{II}} = \tau_c v_c \bar{J}_{\mathrm{II}} = 2J_{\mathrm{IIc}}\bar{J}_{\mathrm{II}} \tag{6a, b}$$

This gives the total ERR $J = J_{\mathrm{I}} + J_{\mathrm{II}}$. As apparent, the fracture energy J_c varies with mode mixity, although the normalised fracture energy remains constant in all modes, i.e. $\bar{J}_c = 1/2$. The normalised

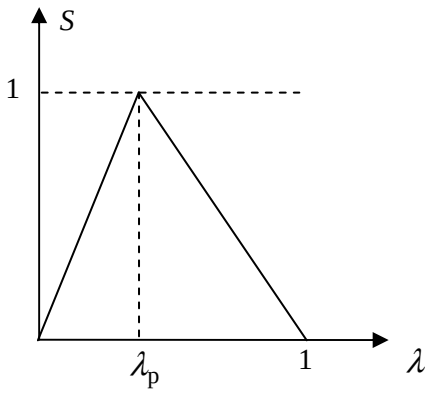

Figure 3 The normalised cohesive law.

normal and tangential stresses are given by

$$\bar{\sigma} = \frac{\sigma}{\sigma_c} = \frac{\partial \bar{J}}{\partial \bar{w}} = \frac{S}{\lambda}\bar{w}, \qquad \bar{\tau} = \frac{\tau}{\tau_c} = \frac{\partial \bar{J}}{\partial \bar{v}} = \frac{S}{\lambda}\bar{v} \tag{7a, b}$$

which gives the mixed mode cohesive behaviour of the adhesive layer, i.e. $\sigma(w,v)$ and $\tau(w,v)$.

3. Interphase elements

The mixed mode cohesive law presented in the previous section is implemented into interphase finite elements that are used in numerical simulations of the unsymmetric DCB-specimen and the MCB-specimen. The interphase elements are 4-node elements with three degrees of freedom in each node to enable structural beam element modelling, i.e. translations in horizontal and vertical directions and the rotation. All the numerical simulations are done using the commercial finite element program ABAQUS 6.4-1, together with a FORTRAN subroutine for the interphase user element. A mid plane is introduced to account for large deformations; this is indicated by the dashed line between the two interfaces.

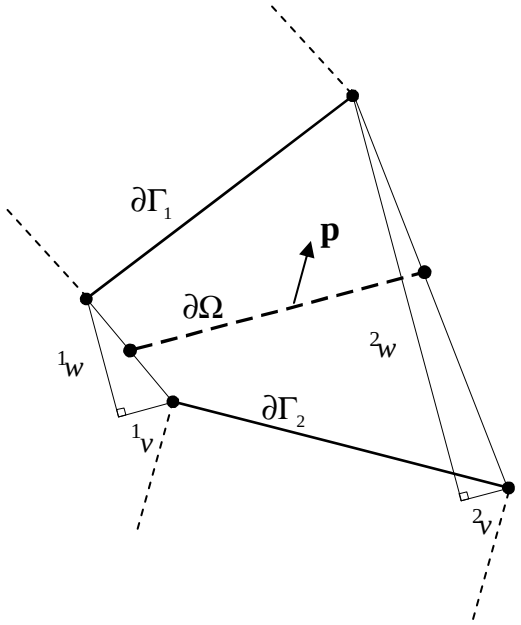

Figure 4 The 4-node interphase element with the adherend cross sectional rotation indicated by dashed lines. Superscripts 1 and 2 indicate over which integration point the relative displacements are measured.

A vector **p** is formed using the normalised stresses in Eq. (7) with the normal and tangential stresses as components according to

$$\mathbf{p} = \begin{bmatrix} \bar{\sigma} \\ \bar{\tau} \end{bmatrix} \tag{8}$$

A metric matrix, **A** transforms the usual basis functions to calculate the correct force at the adherend-adhesive interfaces $\partial\Gamma_1$ and $\partial\Gamma_2$ illustrated in Fig. 4. To achieve the correct relative displacement between interfaces, the heights $t_{(r)}$ are used in Eq. (9) where r = 1,2 indicate each adherend.

$$\mathbf{A}^{(r)} = \begin{bmatrix} 1 & 0 & t_{(r)}/2 \\ 0 & 1 & 0 \end{bmatrix} \qquad \mathbf{N} = \begin{bmatrix} N_1 & 0 & 0 & N_1 & 0 & 0 \\ 0 & N_2 & 0 & 0 & N_2 & 0 \\ 0 & 0 & N_3 & 0 & 0 & N_3 \end{bmatrix} \tag{9a, b}$$

For simplicity, a matrix **G** is created

$$\mathbf{G} = \begin{bmatrix} \mathbf{A}^1\mathbf{N} & -\mathbf{A}^2\mathbf{N} \end{bmatrix} \tag{10}$$

The nodal force vector, **F**, is calculated at the mid plane, $\partial\Omega$ in Eq. (11) below, and then translated to each node for force equilibrium.

$$\mathbf{F} = \int_{\partial\Omega} \mathbf{G}^{\mathrm{T}} \cdot \mathbf{p} \, \mathrm{d}\partial\Omega \tag{11}$$

Moreover, the tangent stiffness matrix **K** is given by

$$\mathbf{K} = \frac{\partial \mathbf{F}}{\partial \mathbf{a}} = \frac{\partial}{\partial \mathbf{a}} \int_{\partial\Omega} \mathbf{G}^{\mathrm{T}} \cdot \mathbf{p} \, \mathrm{d}\partial\Omega = \int_{\partial\Omega} \mathbf{G}^{\mathrm{T}} \cdot \frac{\partial}{\partial \mathbf{u}} \mathbf{p} \frac{\partial}{\partial \mathbf{a}} \mathbf{u} \, \mathrm{d}\partial\Omega \tag{12}$$

where **a** are the local degrees of freedom. The mixed mode constitutive law is found in $\frac{\partial}{\partial \mathbf{u}}\mathbf{p}$, where, as explained previously, **p** incorporates the normalized stress from Eqs. (3) and (7).

4. Simulation of adhesive joints

Two types of specimens for mixed mode testing of adhesive layer are simulated with the layer technique at structure level: the Unsymmetric Double Cantilever Beam (UDCB) and the Mixed mode Cantilever Beam (MCB). The linear elastic adherends are modelled as Euler-Bernoulli beams. The nonlinear constitutive behaviour of the adhesive layer is given by the mixed mode cohesive law in Chapter 2. The adhesive joints are modelled by the layer technique, where the adhesive layer is modelled with the interphase formulation given in Chapter 3.

The cohesive parameters for the adhesive layer are extracted from the experimental results from the DCB-specimen test for mode I and the ENF-specimen test for mode II, cf. Fig. 5. The characteristic cohesive parameters used are

- the fracture energy: J_{Ic} = 0.76 N/mm and J_{IIc} = 2.30 N/mm
- the strength: σ_{c} = 20 MPa and τ_{c} = 26 MPa
- the linear elastic properties: k_{I} = 21.4 GPa/mm and k_{II} = 3.57 GPa/mm

The remaining shape parameters for the saw-tooth model, i.e. the deformation parameters w_{p}, w_{c}, v_{p} and v_{c}, are determined by simple geometry.

The material choice is the same as for the DCB- and ENF-specimen test mentioned previously. The adhesive, DOW Betamate XW1044-3, is a toughened epoxy, with E = 2 GPa and ν = 0.4. The adherends are made of tool steel, with E_1 = 200 GPa, ν = 0.3 and σ_{yield} = 500 MPa.

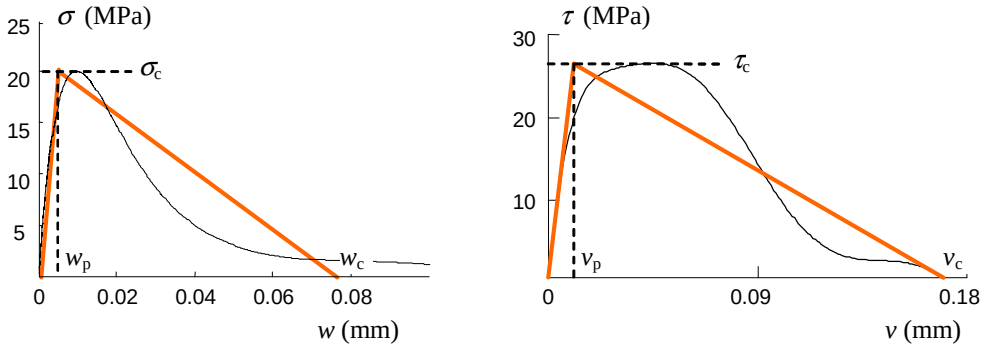

Figure 5 The saw-tooth curve simplifies the cohesive behaviour of an adhesive layer. Pure mode I to the left (Andersson and Stigh, 2004) and pure mode II to the right (Leffler et al., 2006).

4.1 Unsymmetric DCB-specimen

The Double Cantilever Beam (DCB) specimen is a common test geometry. An unsymmetric DCB-specimen (UDCB) has adherends made of the same material but with different thicknesses. Figure 6 shows the crack length a, the overlap length L, and the external peeling force F on an UDCB-specimen. The crack tip is located at $x = 0$. Far from the crack tip, the stress and deformation in the adhesive layer fade out.

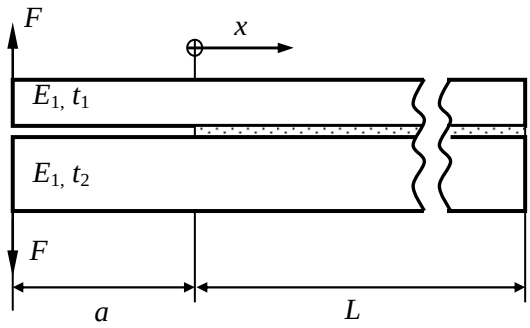

Figure 6 The Unbalanced Double Cantilever Beam (UDCB) specimen.

For an elastic adhesive joint, linear or nonlinear, the J-integral is defined by

$$J = \int_s (W\mathrm{d}y - \mathbf{T}\cdot\frac{\mathrm{d}\mathbf{u}}{\mathrm{d}x}\mathrm{d}s) \tag{13}$$

where $W = \int \boldsymbol{\sigma}\,\mathrm{d}\boldsymbol{\varepsilon}$ is the strain energy density, cf. Rice (1968). The traction vector $\mathbf{T} = \boldsymbol{\sigma}\mathbf{n}$, where $\boldsymbol{\sigma}$ is the stress tensor and $\mathbf{n}$ the unit vector normal and outwards to the counter-clockwise integration path s. The deformation vector and the strain tensor are denoted as $\mathbf{u}$ and $\boldsymbol{\varepsilon}$, respectively.

The ERR of the adhesive joint can be determined by the J-integral if a closed integration path without singularity is chosen, e.g. the path s following the outer boundary as shown in Fig. 7 for the UDCB-specimen. The parts of the path that are not traction-free are situated at the crack tip region, denoted by DA, AB and BC. The J-integral along the closed integration path s, or path AB and BA, yields energetic force equilibrium

$$J = J_{\mathrm{AB}} + J_{\mathrm{BA}} = 0 \tag{14}$$

We first focus on the path AB, which goes through the adhesive layer at the crack tip. The adhesive layer deforms in a combination of two modes: peel (mode I) and shear (mode II). Evaluating the terms in Eq. (13) gives

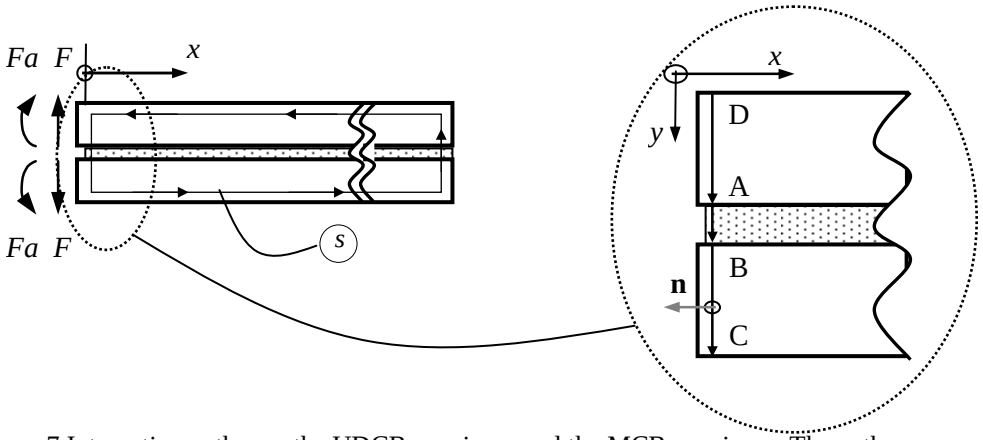

Figure 7 Integration path s on the UDCB-specimen and the MCB-specimen. The path s follows the outer boundary of the specimen and is slightly shrunk for visibility.

$$J_{\mathrm{AB}} = \int_0^{v} \tau \, \mathrm{d}\tilde{v} + \int_0^{w} \sigma \, \mathrm{d}\tilde{w} \tag{15}$$

where τ and σ are the tangential and normal components of the traction, and v and w are the tangential and normal deformation of the adhesive layer through the path AB.

On the path BA, only the paths DA and BC contribute to J_{BA}. Assuming the adherends to deform according to Euler-Bernoulli beam theory, Eq. (13) yields the total ERR due to the load

$$-J_{\mathrm{BA}} = \frac{6}{E_1}\left(\frac{Fa}{b}\right)^2\left(\frac{1}{t_1^3}+\frac{1}{t_2^3}\right)+\frac{F}{b}(w_1'-w_2') \tag{16}$$

where b is the width of the specimen and $w_{1,2}'$ is the rotation of the adherends at the crack tip. All parameters on the right hand side of Eq. (16) are measurable during the experiment.

With the chosen materials mentioned previously, the following dimensions of the UDCB-specimen are used

- Overall joint: L = 100 mm, b = 4 mm, a = 50 mm
- Adhesive: t = 0.2 mm
- Adherends: t_1 = 2 mm, t_2 = 2, 4, …12 mm

In these numerical simulations, the UDCB-specimen has a constant thickness of the upper adherend, t_1 = 2 mm. The thickness of the lower adherend, t_2, varies from 2 to 12 mm, to achieve different mode mixities. When both adherends are equal in thickness, the adhesive layer deforms in pure mode I. An increasing t_2 causes an increase in mode II loading of the adhesive layer. The proportion of the mode II deformations is slightly larger when the adhesive behaves linear elastically. However, for all chosen t_2, the adhesive mainly deforms in mode I. The pure mode II case, cannot be achieved with the UDCB-specimen.

The simulations are performed using a prescribed displacement on the loading points. Figure 8 shows the reaction force, F, and the ERR due to F, J_{BA}, cf. Eq. (16). The loading system is stable, F declines somewhat after reaching the peak value. The ERR, J_{BA}, increases until the fracture energy is reached as a plateau.

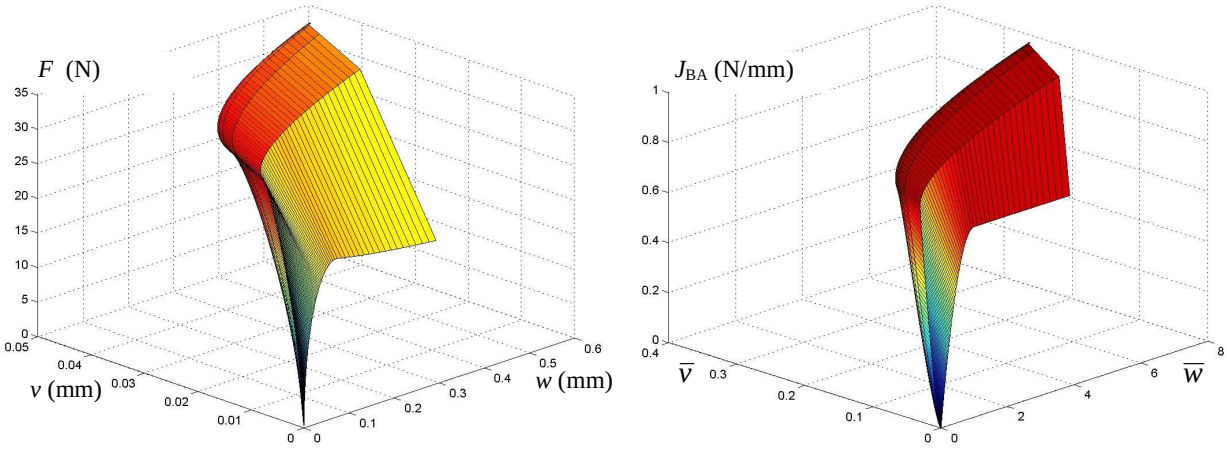

Figure 8 Simulation results on the UDCB-specimen, $F(w,v)$ and $J(w,v)$.

4.2 MCB-specimen

The Mixed-mode double Cantilever Beam (MCB) has a common geometry to a semi-infinite symmetric DCB-specimen. Each adherend, at the free end of the MCB-specimen, is loaded with an external force, F, with the same magnitude but opposite direction. This pair of forces are self-balancing and their direction of action is defined by the angle α, as shown in Fig. 9. The MCB-specimen is designed to

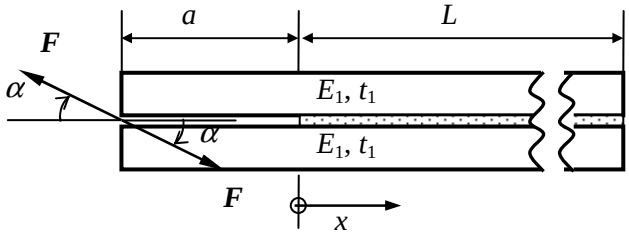

Figure 9 Mixed-mode double Cantilever Beam (MCB) specimen allows the adhesive layer to be loaded in any mode mixities.

achieve the entire spectrum of mode mixity, i.e. from pure mode I to pure mode II. The mode mixity varies steadily by the loading angle α if the crack length a is short (Högberg and Stigh, 2006). With the same integration path s as shown in Fig. 3.2, the total ERR due to the load is

$$-J_{BA} = \frac{12}{E_1 t_1}\left(\frac{F\sin\alpha}{b}\frac{a}{t_1}\right)^2 + \frac{4}{E_1 t_1}\left(\frac{F\cos\alpha}{b}\right)^2 + \frac{F\sin\alpha}{b}(w_1' - w_2') \qquad (17)$$

where $w_{1,2}'$ is the rotation of the adherends at the crack tip, b is the width of the specimen. Here, the adherends are assumed to deform according to Euler-Bernoulli beam theory. All parameters on the right hand side of Eq. (17) are measurable during the experiment.

The same material are used as for the UDCB-specimen, the following dimensions of the MCB-specimen are chosen for simulations

- Overall joint: L = 100 mm, b = 4 mm, a = 0 mm
- Adhesive: t = 0.2 mm
- Adherends: t_1 = 8 mm

The chosen MCB-specimen geometry is simulated with 10 evenly distributed mode mixities: α = [0, π/18…π/2]. The experiments are controlled by prescribed deformation, which increases from zero to 0.4 mm. The results in Fig. 3.5 show that this number of mode mixites is large enough to catch the overall behaviour of the adhesive layer. It is also concluded that the loading system is stable. The reaction forces under the loading point and the deformation of the adhesive layer are measured and plotted in the left graph in Fig. 3.5. The ERR is evaluated by Eq. (17), which is illustrated in the right graph. To reach J_{IIc}, F = 3.8 kN is required. This verifies the results given by the linear elastic analysis for dimensioning the MCB-geometry by Högberg and Stigh (2006).

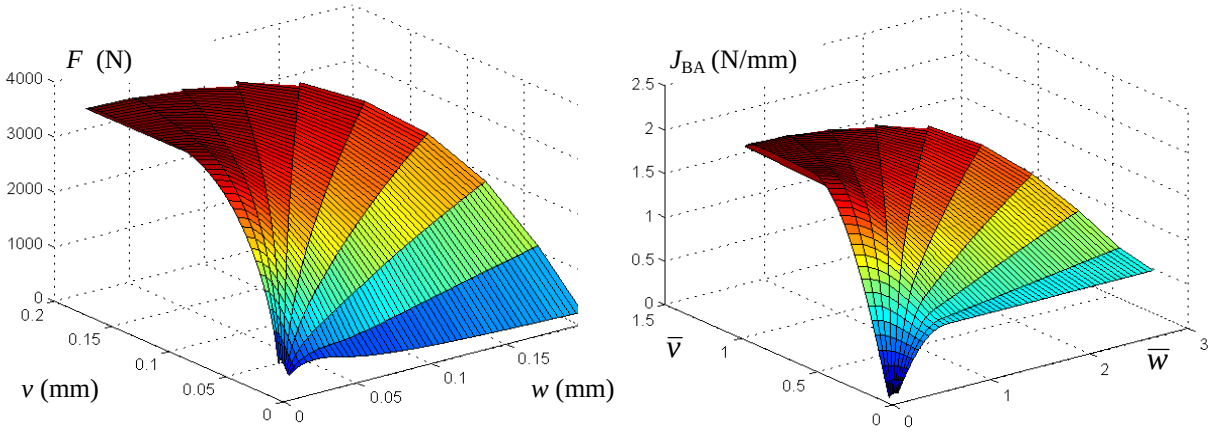

Figure 3.5 Simulation results on the MCB-specimen, $F(w,v)$ and $J(w,v)$.

4 Conclusion

The layer technique is employed to simulate adhesive joint, by which the adhesive layer is modelled as an interphase with a thickness at the macroscopic level. Experimental studies show that the constitutive behaviour of the adhesive layer is nonlinear and mode dependent, which is captured by the mixed mode cohesive law given in Chapter 2. The mixed mode cohesive law has a coupled formulation, and it describes a traction-separation relation that allows for different fracture parameters, such as fracture energy, strength and critical separation in different mode mixities. This cohesive law can also be applied to other fields in fracture mechanics.

For numerical simulations, interphase elements are developed and used to model the adhesive layer. The rotation of the beam adherends is accounted in its large deformation formulation. Examples on FE-implementation of adhesive joints are given. The Unsymmetric Double Cantilever Beam (UDCB) specimen achieves mode mixity by its geometrical unbalance. The Mixed-mode double Cantilever Beam (MCB) specimen achieves the mode mixity by the line of the action of the loading system. The constitutive law of the adhesive layer can be evaluated by the use of the *J*-integral. The results show that the variations in the external force and the ERR in different mode mixities can be recreated, which shows the simplicity and the diversity of the layer technique.

Acknowledgement:

The presented work is a part of co-operation project with the Mechanics of Material group at the Department of Applied Mechanics at Chalmers University of Technology.

References:

Andersson T. and Stigh U. (2004) The stress-elongation relation for an adhesive layer loaded in peel using equilibrium of energetic forces. International Journal of Solids and Structures 41, 413-434.

Barenblatt G.I. (1962) The mathematical theory of equilibrium cracks in brittle fracture. Advances in Applied Mechanics 7, 55-129.

Chai H. (2003) Interfacial mixed-mode fracture of adhesive bonds undergoing large deformation. International Journal of Solids and Structures 40, 6023-6042.

Högberg J.L. (2004) Mechanical behaviour of single-layer adhesive joints – an integrated approach. Thesis for the degree of Licentiate of Engineering, Chalmers University of Technology, Göteborg, Sweden. ISSN 1650-8912 2004:3. (Available at *www.his.se/MechMat*)

Högberg J.L. and Stigh U. (2006) Specimen proposals for mixed mode testing of adhesive layer. Engineering Fracture Mechanics73, 2541-2556.

Högberg J.L. (2006) Mixed mode cohesive law. Accepted for publication in International Journal of Fracture.

Kafkalidis M.S. and Thouless M.D. (2002) The effect of geometry and material properties on the fracture of single lap-shear joints. International Journal of Solids and Structures 39, 4367-4383.

Leffler K., Alfredsson K.S. and Stigh U. (2006) Shear behaviour of adhesive layers. Accepted for publication in International Journal of Solids and Structures.

Li S., Thouless M.D., Waas A.M., Schroeder J.A. and Zavattieri P.D. (2006) Mixed-mode cohesive-zone models for fracture of an adhesively bonded polymer–matrix composite. Engineering Fracture Mechanics 73, 64-78.

Pantano A. and Avrill R.C. (2004) A mesh-independent interface technology for simulation of mixed-mode delamination growth. International Journal of Solids and Structures 41, 3809-3831.

Pardoen T., Ferracin T., Landis C.M. and Delanny F. (2005) Constraint effects in adhesive joint fracture. Journal of the Mechanics and Physics of Solids 53, 1951-1983.

Rice J.R. (1968) A path independent integral and the approximate analysis of strain concentration by notches and cracks. Journal of Applied Mechanics 35, 379-386.

Salomonsson K. (2002) Interphase elements connection structural finite elements formulation, implementation and verification. Master thesis. Chalmers University of Technology, Göteborg, Sweden. (Available at *www.his.se/MechMat*)

Salomonsson K. and Andersson T. (2006) Modeling and calibration of an adhesive layer at the meso level. Submitted for publication.
Sørensen B.F., Jorgensen K., Jacobsen T. K. and Ostergaard R. (2004) A general mixed mode fracture mechanics test specimen: the DCB-specimen loaded with uneven bending moments. Riso-R-1394(EN). Riso National Laboratory, Roskilde, Denmark.
Tvergaard V. and Hutchinson J.W. (1992) The relation between crack growth resistance and fracture process parameters in elastic-plastic solids. Journal of the Mechanics and Physics of Solids 40, 1337-1397.
Tvergaard V. and Hutchinson J.W. (1996) On the toughness of ductile adhesive joints. Journal of the Mechanics and Physics of Solids 44(5), 789-800.